Supporting information

"On the performance of four methods for the numerical solution of ecologically realistic size-structured population models" by Lai Zhang, Ulf Dieckmann, and Åke Brännström

Appendix S1: Illustration of numerical diffusion and numerical instability in transport-dominated PDEs

We demonstrate the potential for undesired numerical diffusion and numerical instability when using a standard finite difference scheme for solving the transport equation

$$\frac{\partial u}{\partial t} + \frac{\partial}{\partial x}(cu) = 0.$$

This equation has an analytical solution of the form $u(x,t) = f(x-ct)$. Consider the initial condition

$$u(x,0) = g(x) = \begin{cases} 1 & 0 \le x \le 10, \\ 0 & \text{otherwise.} \end{cases}$$

We see that the solution to the transport equation is

$$f(x-ct) = \begin{cases} 1 & 0 \le x - ct \le 10, \\ 0 & \text{otherwise.} \end{cases}$$

The solution is discontinuous and consequently has sharp changes, which makes numerical approximation challenging.

One problem that can arise when solving transport equations is numerical diffusion. Fig. S1 shows that numerical diffusion appears when a standard finite difference upwind scheme is employed. Due to the numerical diffusion, the numerical solution is smoother and fails to accurately capture the large changes. This undesired numerical diffusion continues to smoothen out the numerical solution as time progresses.

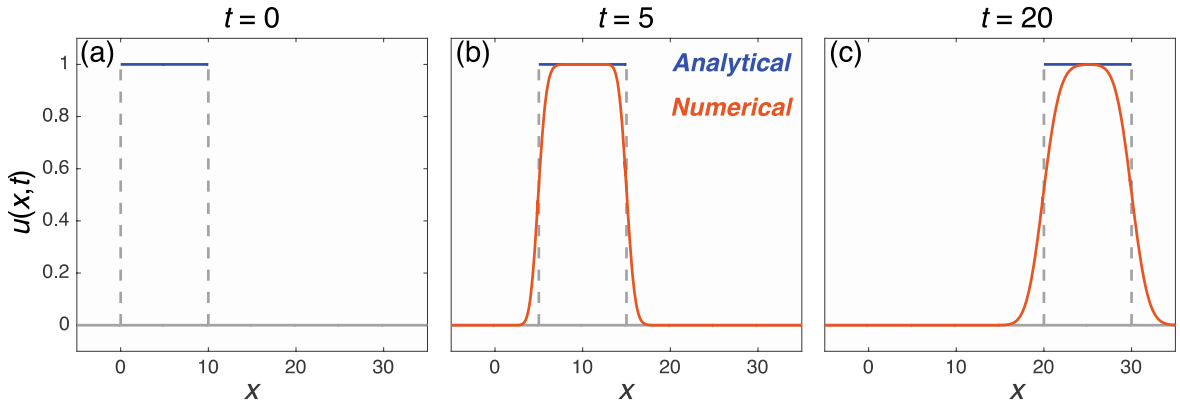

Fig. S1: Numerical diffusion causes the numerical solution to become smoother over time, even though the analytical (correct) solution remains discontinuous, with sharp changes. The analytical and numerical solution are presented for the given transport equation with $c = 1$, at time $t = 0$ (initial condition; panel a), $t = 5$ (panel b), and $t = 20$ (panel c). The numerical solution was obtained using the first order upwind scheme (Patankar, 1980) with 401 mesh points over the range from $x = -5$ to $x = 35$, and a time-step size of 0.01.

Another problem that can arise when solving transport equations is numerical instability. Fig. S2 shows spurious oscillations that appear when the standard centered finite difference scheme is employed. As numerical instability can easily arise when using standard finite difference schemes, we recommend an upwind scheme for solving transport equations.

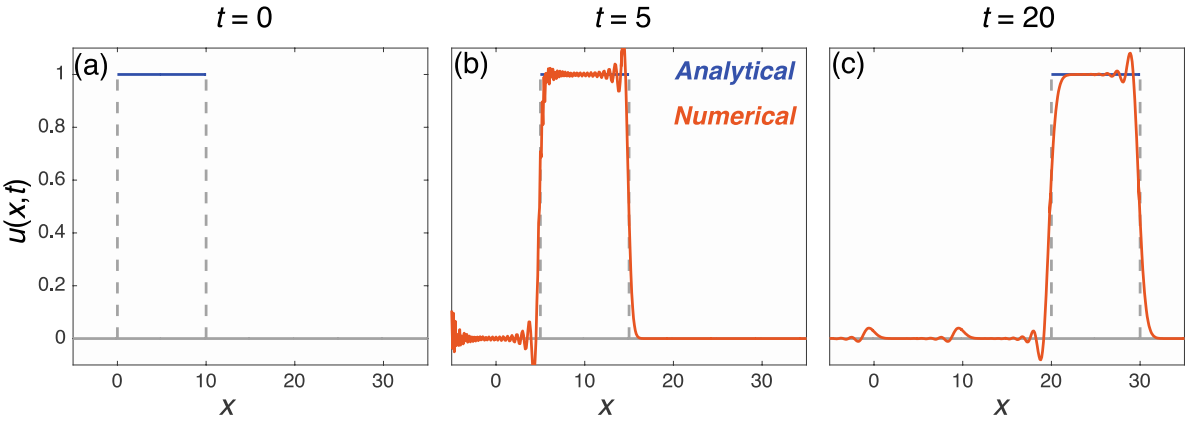

Fig. S2: Numerical instability causes spurious oscillations in the computed numerical solution. The numerical solution was obtained using the standard first-order centered finite difference scheme. The panels and parameter values are the same as in Fig.S1.

Appendix S2: Description of the fixed-mesh upwind method

In both the fixed-mesh upwind method (FMU) and the moving-mesh upwind method (MMU), the size range (i.e., $[x_{\mathrm{b}}, x_{\mathrm{m}}]$) is partitioned into a number of non-overlapping intervals and the PDE is transformed to a set of ODEs following a bookkeeping argument. We first allow the mesh points to depend on time for the convenience of later use. The FMU method is recovered by assuming a fixed mesh. We note that the FMU method presented here is similar to the box method in Angulo and Lopez-Marcos (2002).

We consider J disjoint intervals denoted by $[x_i(t), x_{i+1}(t)]$ ($i = 1, \cdots, J$) with $x_1(t) = x_{\mathrm{b}}$ and $x_{J+1}(t) = x_{\mathrm{m}}$. Integrating equation (1a) over the interval $[x_i(t), x_{i+1}(t)]$ and reorganizing the resulting equation, we have

$$\frac{\mathrm{d}}{\mathrm{d}t}\int_{x_i}^{x_{i+1}} u(x,t)\,\mathrm{d}x = -\int_{x_i}^{x_{i+1}} \mu(x,E_t)\,u(x,t)\mathrm{d}x - \left[\left(g(x,E_t) - \frac{\mathrm{d}x}{\mathrm{d}t}\right)u(x,t)\right]_{x_i}^{x_{i+1}}, \qquad \text{(S1)}$$

where the left-hand side represents the change in number of individuals in the i-th interval while the first and second term on the right-hand side, respectively, represent the number of individuals that are removed from the interval due to mortality and the net number of individuals that leave or enter the interval due to growth. For $i = 1$, $g(x_1, E_t)u(x_1, t)$ will be evaluated by the integral in equation (1b)to account for newborn individuals.

We define the interval average as

$$U_i = \frac{1}{x_{i+1}-x_i}\int_{x_i}^{x_{i+1}} u(x,t)\,\mathrm{d}x$$

and then equation (S1) can be rewritten as

$$h_i(t)\frac{\mathrm{d}U_i}{\mathrm{d}t} = -\int_{x_i}^{x_{i+1}} \mu(x,E_t)u(x,t)\mathrm{d}x - \left[\left(g(x,E_t) - \frac{\mathrm{d}x}{\mathrm{d}t}\right)u(x,t)\right]_{x_i}^{x_{i+1}} - \frac{\mathrm{d}h_i}{\mathrm{d}t}U_i(t), \qquad \text{(S2)}$$

where $h_i(t) = x_{i+1}(t) - x_i(t)$ is the width of the i-th interval at time t, and the last term accounts for the way in which interval average changes with interval width.

Clearly, we have to approximate the integrals appearing in equation (S2) and in the nonlocal boundary condition (1b). By the midpoint quadrature rule, they can be approximated as

$$\int_{x_i}^{x_{i+1}} \mu(x,E_t)\,u(x,t)\mathrm{d}x = h_i(t)\mu(X_i,E_t)U_i$$

$$\int_{x_0}^{x_m} \beta\,(x,E_t)u(x,t)\mathrm{d}x = \sum_{i=1}^{i=J} h_i(t)\,\beta(X_i,E_t)U_i(t)$$

where $X_i = (x_i(t) + x_{i+1}(t))/2$ is the middle point of the i-th interval.

To approximate the flux term in equation (S2), we derive estimates of the densities at the interval boundaries, i.e., of $u_i = u(x_i, E_t)$, from the average densities of the two neighboring intervals. There are several ways to estimate the densities at the interval boundaries, and we employ the first order upwind method with a superbee flux limiter (Roe, 1986). This scheme is up to second order accurate and has the advantage of being numerically stable as well as free of spurious oscillations. Specifically,

$$\mathrm{u}(x_\mathrm{i}) = \begin{cases} U_{i-1} + \phi(r_i^-)(U_{i-1} - U_{i-2})\frac{x_i - x_{i-1}}{x_{i+1} - x_{i-1}} & \text{if} \quad g(x_i) - \frac{\mathrm{d}x_i}{\mathrm{d}t} \geq 0, \\ U_i - \phi(r_i^+)(U_{i+1} - U_i)\frac{x_{i+1} - x_i}{x_{i+2} - x_i} & \text{otherwise,} \end{cases}$$

where $\mathrm{u}(x_\mathrm{i})$ is used in equation (S2), and

$$\phi(r) = \max\{0, \min\{2r, 1\}, \min\{r, 2\}\},$$

and

$$r_i^- = \frac{(U_i - U_{i-1})(x_i - x_{i-2})}{(U_{i-1} - U_{i-2})(x_{i-1} - x_{i-2})}, \text{ and } r_i^+ = \frac{(U_{i-1} - U_i)(x_i - x_{i+2})}{(U_i - U_{i+1})(x_{i-1} - x_i)}.$$

The FMU method is recovered by setting $\mathrm{d}x/\mathrm{d}t = 0$, as a consequence of which the last term in equation (S2) vanishes.

The FMU method as implemented here differs from the first-order upwind schemes (FOU) in the approximation of the fluxes at the boundaries of size classes. The FOU methods are numerically stable but have low accuracy in each step. By contrast, higher-order upwind schemes such as the third order QUICK scheme (Leonard, 1979) have high accuracy in each step but are susceptible to spurious oscillations over several steps (LeVeque, 2002). In an effort to combine the best of features of both, we employ a "flux limiter" which interpolates between first-order and higher-order methods depending on local properties of the solution, typically the gradient (Sweby, 1984; Roe, 1986). Specifically, we have adopted the so-called superbee flux limiter by Roe (1986), which together with the second order upwind scheme has been demonstrated to be able to effectively suppress spurious oscillations (LeVeque, 2002). The superbee flux limiter is used in both the FMU and MMU method.

Appendix S3: Description of the moving-mesh upwind method

The MMU method is identical to the FMU method except that mesh points are dynamic (i.e., $\mathrm{d}x/\mathrm{d}t \neq 0$). Thus, only the way of moving mesh points has to be specified. Here we employ

a moving mesh technique that has been widely used in computational fluid dynamics (Huang and Russel, 2011). The idea is to choose a measure of mesh "badness" and place the mesh points in such a way that each interval has the "same amount" of badness. This can be achieved by using a so-called monitor function $\rho(x,t)$. The mesh points are moved to reduce the distances between mesh points in regions with higher $\rho(x,t)$, and to increase the distances between mesh points in regions with smaller $\rho(x,t)$, known as the equidistribution principle (de Boor, 1973). Based on this principle, the dynamics of node points are governed by the following ODEs,

$$\rho_{i+\frac{1}{2}}\left(\frac{\mathrm{d}x_{i+1}}{\mathrm{d}t}-\frac{\mathrm{d}x_i}{\mathrm{d}t}\right)-\rho_{i-\frac{1}{2}}\left(\frac{\mathrm{d}x_i}{\mathrm{d}t}-\frac{\mathrm{d}x_{i-1}}{\mathrm{d}t}\right)=-\frac{1}{\tau}\left(\rho_{i+\frac{1}{2}}(x_{i+1}-x_i)-\rho_{i-\frac{1}{2}}(x_i-x_{i-1})\right) \quad \text{(S3)}$$

for $2 \leq i \leq J$. The boundary points are fixed throughout simulation, that is, $\mathrm{d}x_1/\mathrm{d}t = 0$ and $\mathrm{d}x_{J+1}/\mathrm{d}t = 0$. Here, $\rho_{i+1/2}$, is defined as $\rho_{i+1/2} = (\rho_{i+1}+\rho_i)/2$ with $\rho_i = \rho(x_i,t)$. There is a user-specified temporal regularization parameter τ in equation (S3), which is used to adjust the response time of mesh movement to the change in $\rho(x,t)$. The larger τ, the more slowly the meshes move, and vice versa (see subsection ***Impact of monitor function***). The moving mesh equation (S3) is called MMPDE4, one of a number of moving mesh equations in Huang et al. (1994). Our choice is recommended for use in hyperbolic systems (Stockie et al., 2001).

The key to the success of the proposed method is to choose an appropriate monitor function. We base our choice on the arc-length function (Huang and Russell, 2011)

$$\rho(x,t)=\sqrt{1+\frac{1}{\alpha}\left(\frac{\partial}{\partial x}u(x,t)\right)^2}\,. \quad \text{(S4a)}$$

Our monitor function equidistributes the arc-length of the approximated individual size-distribution, and allocates more points to the regions with high gradient, which usually require very refined mesh to enhance accuracy. To avoid that excessive points are attracted to the areas with steep gradient, the regularizing factor

$$\alpha=\frac{1}{x_m-x_b}\int_{x_b}^{x_m}\left(\frac{\partial}{\partial x}u(x,t)\right)^2\mathrm{d}x$$

is introduced, which scales the derivative term by its average value over the considered size-distribution. This factor α allows one to reduce the magnitude of the monitor function in situations where the solution gradient is very large, thereby avoiding over-resolution of steep

layers, while also ensuring that the monitor function still retains a significant peak near the region of high solution gradient.

The monitor function (S4a) works quite well for a large class of SSPMs, for instance our test Daphnia and fish model. However, for the test vegetation model, due to the strong asymmetric competition affecting growth rates, two sharp peaks in the individual size-distribution appear around the smallest and largest size. As the abundance of the largest individuals is several orders lower than that of the smallest individuals, the monitor function (S4a) will place fewer mesh points near the maximum size than what would be needed for high numerical accuracy. In this case, a function monitoring both density and biomass improves the ability of capturing sharp profiles (see subsection ***Impact of monitor function***). This can be formulated as

$$\rho(x,t) = \frac{1}{2}\sqrt{1+\frac{1}{\alpha}\left(\frac{\partial}{\partial x}u(x,t)\right)^2} + \frac{1}{2}\sqrt{1+\frac{1}{\alpha}\left(\frac{\partial}{\partial x}u_B(x,t)\right)^2}, \tag{S4b}$$

where $u_B(x,t)$ is the biomass distribution over size x at time t (Stockie et al., 2001). The corresponding smooth version of this function is employed for testing this method with vegetation model.

It is well-known that some sort of smoothing of the mesh is required in order to maintain reasonable accuracy in the computation of a solution on an adaptive mesh. A commonly applied technique in the moving mesh framework is to replace $\rho_{i+1/2}$ by

$$\tilde{\rho}_{i+1/2} = \sqrt{\sum_{k=i-p}^{i+p} \rho_{k+\frac{1}{2}}^2 \left(\frac{\gamma}{1+\gamma}\right)^{|k-i|} / \sum_{k=i-p}^{i+p} \left(\frac{\gamma}{1+\gamma}\right)^{|k-i|}}, \tag{S5}$$

where p and γ are positive integers. The $\tilde{\rho}_{i+1/2}$ can be thought of as a weighted average of its neighbours with the aim to eliminate local oscillatory behavior that may arise from solving the equation (S3) (Stockie et al., 2001).

The equation (S2) and the moving mesh equation (S3) form a tightly coupled nonlinear system, the solution of which demonstrates the coevolution of interval width and abundance over time, which can be solved simultaneously. This method involves a temporal smoothing parameter τ, and two spatial smoothing parameters p, and γ. As numerical performance is much less sensitive to the spatial smoothing, we choose $p = 4$ and $\gamma = 2$ (Stockie et al., 2001). Numerical experiments show that $\tau = 1$ gives good performance (see subsection ***Impact of monitor function***) and we fix the parameter at this value throughout simulations.

Impact of monitor function

We here explore the impacts of the numerical parameter τ and the choice of monitor function (Eq. S4a) and (Eq. S4b) on the mesh distribution.

Figure S3 illustrates how different values of τ affect mesh distribution. The temporal regularization parameter τ influences how quickly the mesh responds to changes in the solution. The smaller the value of τ, the more rapid the response becomes. Quicker response means less numerical diffusion and consequently higher accuracy. However, too small values of τ can make the ODE system (Eq. S3) very stiff, which requires excessively small time over which the mesh relaxes towards equidistribution to avoid mesh oscillations. How to choose a suitable value of τ remains an open question even in computational fluid dynamics (Stockie et al., 2001). However, in our test models, the choice of $\tau = 1$ gives fairly good performance (Fig. S4).

Figure S5 demonstrates the differential abilities of the density monitor function and the density-biomass monitor function for resolving steep gradients in individual size-distributions. We conclude that the latter monitor function performs better for our reference problems. The individual size-distribution clearly shows that the highest gradient occurs at the smallest individuals. This dominance makes the density monitor function unable to effectively detect the sharpness around the largest individuals. However, the biomass distribution over size demonstrates that the solution gradients around the smallest and largest individuals are roughly on the same order. Thus, by monitoring density and biomass distributions simultaneously, the two steep layers can be effectively captured.

The MMU method can perform well only when an appropriate monitoring function is chosen. For most SSPMs, the arc-length density monitor function (Eq. S4a) appears to work very well. In the test vegetation model, a combination of density and biomass monitor functions (Eq. S4b) works well to resolve the two sharp fronts arising due to the aggregations of the small and large individuals. Three parameters jointly specify the monitor functions that we have used. The spatial smoothing parameters (p and γ in Eq. S5) are easy to select as the results are relatively insensitive to their particular values (Stockie et al., 2001). The temporal smoothing parameter (τ in Eq. S3) is harder to choose and numerical experiments are required. Too

much smoothing prevents the moving mesh technique from recognizing a sharp change, resulting in a mesh that is nearly uniform (Fig. S3), while too little smoothing may requires excessively small time steps to meet the error tolerance, making the system of ordinary differential equations that describe the mesh stiff. In the latter case, temporal oscillation in mesh may arise. Surprisingly, while the parameter τ is critical for the computational efficiency of the MMU method, the numerical accuracy of the solution appears insensitive to the choice of τ (Fig. S4).

Appendix S4: Description of the characteristic method

The method solves the partial differential equation (1a) along characteristic curves on which the equation reduces to an ordinary differential equation. The equations for the characteristic curves and for the density $u(x(t),t)$ are

$$\frac{\mathrm{d}x(t)}{\mathrm{d}t} = g(x(t), E_t), \tag{S6a}$$

$$\frac{\mathrm{d}}{\mathrm{d}t}u(x(t),t) = -\big(\mu(x(t),E_t) + g_x(x(t),E_t)\big)u(x(t),t). \tag{S6b}$$

Note that the system is coupled through the environmental feedback E_t, which together with the ordinary differential equations needs to be approximated before a complete numerical scheme is obtained. Numerically we have a finite set of characteristic curves $x_i(t)$ $(i = 1,\cdots,J+1)$ with $x_i(0) = x_b$. The solution $u_i(x_i(t),t)$ or simply denoted by $u_i(t)$, is computed along with $x_i(t)$ on these curves by solving ordinary differential equations.

The equations (S6) are integrated simultaneously for a time interval, Δt, and then a new characteristic curve $x_0(t+\Delta t)$ is introduced to accommodate newborn individuals. The newly added characteristic curve has initial position x_b and density $u_0(t+\Delta t)$ which is determined by the boundary condition (1b). As the environment is globally dependent on the density $u(t+\Delta t)$ including $u_0(t+\Delta t)$, the initial density $u_0(t+\Delta t)$ is found by applying fixed-point iteration to the boundary equation (1b) (Angulo and Lopez-Marcos, 2004). Once the initial density is obtained, the dynamics unfold according to equations (S6).

Due to the frequent addition of new characteristic curves, the number of characteristic curves increases linearly over time. The increasing amount of the ordinary equations makes computation excessively expensive, but this can be avoided by means of a selection of characteristic curves at each time step. As described by Angulo and Lopez-Marcos (2004), to maintain a

constant number of characteristic curves, we keep the first and last characteristic curves but remove an interior curve x_i after each regular time interval Δt, where i is chosen to satisfy

$$|x_{i+1} - x_{i-1}| = \min_{1 \le j \le J} |x_{j+1} - x_{j-1}|.$$

In this method and the EBT method below, numerical experiments are needed to find an appropriate value for Δt. The choice of this value is greatly affected by the number of characteristic curves. In general, small number of characteristic curves (cohorts) requires less frequent internalization of boundary curve (cohort.) Otherwise, a characteristic curve (cohort) that is still playing an important role in population dynamics might have to be removed or deleted in order to keep constant number of curves (cohort). If this situation happens, larger errors in approximating life-history functions can occur, leading to non-physical oscillations. In our simulations, whenever doubling characteristic curve (cohort) number, we halve Δt.

Appendix S5: Description of the Escalator Boxcar Train method

We give a brief description of the method while referring to de Roos et al. (1992) for the specific details. Unlike the characteristic method, the EBT method divides the population into a certain number of cohorts and tracks the mean size as well as the total abundance of each cohort. Specifically, assume that there are internal cohorts N_i with the mean size x_i ($i = 1, \cdots, J$) at time t, and dynamics are described by

$$\frac{\mathrm{d}N_i}{\mathrm{d}t} = -\mu(x_i, E_t)N_i, \tag{S7a}$$

$$\frac{\mathrm{d}x_i}{\mathrm{d}t} = g(x_i, E_t), i = 1, \cdots, J. \tag{S7b}$$

Apart from these internal cohorts, a boundary cohort N_0 is required to account for offspring of mature individuals. For this particular cohort, instead of tracking the mean size the EBT method tracks the cumulative amount π_0 by which the individuals in the boundary cohort exceed their birth size x_b. The dynamics of the boundary cohort are

$$\frac{\mathrm{d}N_0}{\mathrm{d}t} = \mu(x_\mathrm{b}, E_t)N_0 - \mu_x(x_\mathrm{b}, E_t)\pi_0 + \textstyle\sum_{i=0}^{i=J} b(x_i, E_t), N_i, \tag{S8a}$$

$$\frac{\mathrm{d}\pi_0}{\mathrm{d}t} = g(x_\mathrm{b}, E_t)N_0 + g_x(x_\mathrm{b}, E_t)\pi_0 - \mu_x(x_\mathrm{b}, E_t)\pi_0, \tag{S8b}$$

where the summation term indicates the reproduction contribution from the internal cohorts. If the boundary cohort is nonempty the mean size is then defined as $x_0 = x_\mathrm{b} + \pi_0/N_0$. The terms g_x and μ_x mean the first order derivative of growth rate and mortality at size x_b.

The boundary cohort should be internalized sufficiently often to avoid large approximation error resulting from the increased size of this cohort. This is done by the following renumbering procedure at regular time steps Δt,

$$\begin{aligned} N_{i+1}(t+\Delta t^{+}) &= N_i(t+\Delta t^{-}), \\ x_{i+1}(t+\Delta t^{+}) &= x_i(t+\Delta t^{-}), \\ N_1(t+\Delta t^{+}) &= N_0(t+\Delta t^{-}), \\ x_1(t+\Delta t^{+}) &= x_b + \frac{\pi_0(t+\Delta t^{+})}{N_0(t+\Delta t^{+})}, \\ N_0(t+\Delta t^{+}) &= 0\,, \\ \pi_0(t+\Delta t^{+}) &= 0. \end{aligned} \tag{S9}$$

After this operation the number of cohorts is incremented to $J+1$. Additionally, to relive computational load, a cohort with the lowest abundance is removed if its abundance is below a threshold value (10^{-10} is used in our simulations).

Appendix S6: Specification of the Daphnia model

The Daphnia model originates from Kooijman and Metz (1984). It describes a length-structured population (i.e., the water flea *Daphnia magna*) feeding on a dynamical food-source (i.e., algae). Model components and parameters are summarized in Table S1 and S2, respectively.

In this model individual Daphnia is characterized by its length l ranging from the size-at-birth l_b to the maximum size l_m (E1) that can be attained under unlimited food availability ($S(t)$). It is assumed that the surface area and the weight of individuals are proportional to the square and cubic of their lengths, respectively. Under these assumptions, the food-intake rate is then supposed to be the second power of individual length (E2) and additionally follows the Holling type II function response with respect to the resource (E3). The ingested energy is allocated in a constant ratio κ and $1-\kappa$ to individual growth and maintenance on one hand (E4), and reproduction and maturation on the other (E5). Moreover, reproduction occurs only when individuals reach the maturation size l_j. In case that the ingested energy for growth and maintenance is insufficient to cover maintenance alone, individual growth is stunted. In addition, energy allocation is redistributed in such a way that the maintenance requirements are just satisfied and the remaining energy is channeled to maturation as well as reproduction.

Individual suffers from a constant natural mortality (E6) and an instant death rate when the ingested energy is unable to cover maintenance costs.

In the present paper we use a simplified version of the Daphnia model as this allows us to obtain the analytical equilibrium solution. The simplified model was introduced by de Roos (1988) by making two assumptions: First, individuals can shrink in size when starving and will not die from starvation (E7). Second, individuals are allowed to reproduce immediately after they are born (E8). Consequently, individuals only die from natural mortality (E9). After making the two simplifying assumptions, the steady state can be found analytically. For simplicity, the size is scaled to range from 0 to 1 and the resource is assumed to grow logistically in the absence of predation (E10).

Appendix S7: Specification of the fish model

The model is derived from the food-web model with continuously size-structured populations by Hartvig et al. (2011). We consider only one structured consumer feeding on an unstructured resource. Model equations and parameters are summarized in Table S3 and S4, respectively. Below, briefly describe the model. For a detailed explanation, we refer to Hartvig et al. (2011).

Predation is size selective (M1) and the size-based predation upon resource and other consumer individuals provides w sized individuals with the encountered food (M2). Saturation is described by the feeding level (M3), which multiplied with the maximum food intake (M4) gives rise to the ingested food. With an assimilation efficiency α, ingested food is converted to energy (M5) that is utilized for life-history processes. Energy is in priority used for paying maintenance costs $k_s w^p$ and then, if there is any, used for individual somatic growth (M6) and reproduction (M7). The distribution of the remaining energy between these two processes is governed by an allocation function (M8). The growth equation indicates that the surplus energy after paying metabolic cost is entirely used for juvenile growth but drops due to the onset of reproduction. Individuals' growth ceases when they approach the maximum body size M where all energy is routed to reproduction. Mortality (M9) is due to predation (M10), background death i.e., $\mu_0 m^{n-1}$, and starvation (M11) when assimilated energy is insufficient to cover metabolic costs. The maturation size of individuals is denoted by m. Resource is non-structured but continuously size distributed, following the semi-chemostatic growth (M12)

with a carrying capacity (M13) and an intrinsic growth rate (M14). In our test, we choose $m = 1$.

Appendix S8: Specification of the single-patch vegetation model

The vegetation model is a simplification of the metapopulation model of Falster et al (2010) by reducing the spatially implicit multiple patches to a single patch. This is achieved by excluding the reproduction contribution from the patches other than the focusing one. We give a brief depiction of the main life histories and refer readers to Falster et al. (2010) for detailed description. Model equations and parameters are, separately, summarized in Table S5 and S6.

A plant is assumed to have the following components: leaf area (N1), individual height (N2), as well as the mass of its sapwood (N3), heartwood (N4), bark (N5) and roots (N6). All components are allometrically scaled with mass of leaf *m*, the structural variable. As such, dynamic of the plant is reflected via the ontogenetic physiological change of leaves. Moreover, by assuming a constant crown-shape relationship (N7 and N8), the vertical leaf-area distribution over height, combining with the individual size-abundance distribution, gives rise to the cumulated shading level down through the canopy (N9). At different light level, integrating instantaneous photosynthetic rates over its leaf area, the gross carbon-dioxide assimilation is obtained for each individual (N10). The CO_2 gain is depleted first by maintenance respiration (N11) and tissue turnover (N12). The remaining, net dry-matter production (N13), is then allocated to growth (N14, N17) and reproduction (N15, N18). The allocation closely follows the bang-bang strategy (N16), that is, allocation to reproduction changes rapidly at maturation height. Mortality (N19) stems from two sources: intrinsic mortality and growth-related mortality that vary among individuals according to the net mass production per unit leaf area.

Appendix S9: Analytical equilibrium of the size-structured Daphnia model

We here consider the equilibrium solution to the Daphnia model. At equilibrium, the realized maximum body size is determined by $x^* = S^*/(1 + S^*)$. We define the up to third order momenta of the original density as follows

$$N_i(t) = \int_0^1 x^i \, u(t,x)\mathrm{d}x, i = 1, 2.$$

Then we have the following balance equations

$$0 = rS\left(1 - \frac{S}{K}\right) - \frac{S}{1+S}N_2,$$

$$0 = \frac{\alpha S}{1+S}N_2 - \mu N_0,$$

$$0 = \frac{S}{1+S}N_0 - (1+\mu)N_1,$$

$$0 = \frac{2S}{1+S}N_1 - (2+\mu)N_2.$$

Here the first and second equations are derived from the resource equation (E10 in Table S1) and the boundary condition (1b). Multiply equation (1a) with *x* and integrate both sides from 0 to x^* by part. Recall that the growth rate at x^* is zero, reorganizing the resulting equation, we obtain the third balance equation. Similarly, we can derive the last balance equation by multiplying equation (1a) with x^2.

Solving above balance equations yields

$$S^* = \frac{x^*}{1-x^*}, N_0^* = \frac{\alpha x^* N_2^*}{\mu}, N_1^* = \frac{x^* N_0^*}{1+\mu}, N_2^* = rS^*(1 - S^*/K)/x^*,$$

where

$$x^* = \left(\frac{\mu(1+\mu)(2+\mu)}{2\alpha}\right)^{1/3}.$$

Thus the equilibrium size distribution $u^*(x)$ can be obtained by solving equation (1a)

$$u^*(x) = \frac{\alpha r S^*\left(1 - \frac{S^*}{K}\right)}{(x^*)^\mu}(x^* - x)^{\mu-1}, 0 \le x \le x^*.$$

Table S1: Life history elements of the size-structured Daphnia model.

No.	Equation	Interpretation
Original version from Kooijman and Metz (1984)		
E1	$l_{\mathrm{m}} = \kappa v_e/\zeta$	Maximum length
E2	$I(S,l) = v_x f(S) l^2$	Food intake rate
E3	$f(s) = \xi S/(1+\xi S)$	Type II functional response
E4	$g(S,l) = \gamma(l_{\mathrm{m}} f(S) - l)$ for $l < l_{\mathrm{m}} f(s)$	Maximum food intake
E5	$b(S,l) = \begin{cases} 0 & l_b \le l < l_j \\ r_{\mathrm{m}} f(S) l^2 & l_j \le l < l_{\mathrm{m}} f(S) \\ \frac{r_{\mathrm{m}}}{1-\kappa}(f(S) l^2 - \kappa l^3/l_{\mathrm{m}}) & \text{otherwise} \end{cases}$	Individual birth rate
E6	$d(S,l) = \begin{cases} \mu_0, & l < l_{\mathrm{m}} f(S)/\kappa \\ \infty, & \text{otherwise} \end{cases}$	Individual mortality rate
Simplified version from de Roos (1988), used in the present paper		
E7	$g(x,t) = \max(S(t)/(1+S(t)) - x, 0)$	Individual growth rate
E8	$\beta(x,t) = \alpha x^2 S(t)/(1+S(t))$	Individual birth rate
E9	$\mu(x,t) = \mu_0$	Individual mortality rate
E10	$\mathrm{d}S(t)/\mathrm{d}t = rS(1-S/K) - \frac{S}{1+S}\int_0^1 x^2 u(x,t)\mathrm{d}x$	Resource dynamics

Table S2: Parameter values of the size-structured Daphnia model

Parameter	Value	Unit	Description
l_b	0.8	mm	Length at birth
l_j	2.5	mm	Length at maturation
l_m	6	mm	Maximum length
κ	0.3	–	Fraction of ingested energy channeled to growth and maintenance
v_x	1.8×10^6	cell mm^{-2} day^{-1}	Maximum feeding rate per unit surface area
γ	0.15	day^{-1}	Time constant of growth
ξ	7.0×10^{-6}	ml $cell^{-1}$	Shape parameter of the functional response
r_m	0.1	$mm^{-2} day^{-1}$	Maximum reproduction rate per unit surface area
α	0.75	–	Scaled reproduction rate
μ_0	0.1	day^{-1}	Natural mortality rate
r	0.5	day^{-1}	Intrinsic growth rate for resource[a]
K	3	cell ml^{-1}	Resource carrying capacity[a]

[a]Chosen to ensure stable steady state. The remaining are from Kooijman and Metz (1984) and de Roos et al. (1990).

Table S3: Life history elements of the size-structured fish model

No.	Equation	Interpretation
M1	$\varphi\left(\frac{w}{w'}\right) = \exp(-\log^2\left(\frac{w'\beta}{w}\right)/(2\sigma^2))$	Selection function
M2	$E(w) = \gamma w^q \left(\int_0^{m_{\text{cut}}} w'\, R(w')\varphi\left(\frac{w}{w'}\right) dw' + \sum_j \int_{w_0}^{\frac{m_j}{\eta}} w'\, N_j(w')\varphi\left(\frac{w}{w'}\right) dw'\right)$	Encountered food from resource and consumer
M3	$F(w) = E(w)/(E(w) + I_{\max}(w))$	Feeding level
M4	$I_{\max}(w) = hw^n$	Maximum food intake
M5	$S(w) = \alpha I_{\max}(w) F(w)$	Assimilated energy
M6	$\psi(w,m) = (1 + (w/m)^{-10})^{-1}(w\eta/m)^{1-n}$	Allocation function
M7	$g(w,m) = \max\{0, \big(1 - \psi(w,m)\big)S(w) - k_s w^p\}$	Individual growth rate
M8	$b(w,m) = \max\{0, \psi(w,m)(S(w) - k_s w^p)\}$	Individual birth rate
M9	$\mu_p(w) = \sum \int_{w_0}^{M_j} \nu(w')\big(1 - F(w')\big)N_j(w')\varphi(w'/w)dw'$	Predation mortality
M10	$\mu_s(w) = \max\{(S(w) - k_s w^p)/(\xi w), 0\}$	Starvation mortality
M11	$\mu(w) = \mu_p(w) + \mu_0 m^{n-1} + \mu_s(w)$	Mortality rate
M12	$dR/dt = r(w)(\kappa(w) - R) - \mu_p(w)$	Resource dynamics
M13	$\kappa(w) = \kappa_0 w^{-\lambda}$	Resource carrying capacity
M14	$r(w) = r_0 w^{-\lambda}$	Resource growth rate

Table S4: Parameter values of the size-structured fish model

Parameter	Value	Unit	Description
β	100	−	Preferred predator-prey mass ratio
σ	1	−	Width of selection function
α	0.6	−	Assimilation efficiency
ε	0.1	−	Reproduction efficiency
h	85	g/year	Scaled prefactor of maximum food intake
k_s	10	g/year	Scaled prefactor of standard metabolism
n	0.75	−	Exponent of maximum food intake
p	0.75	−	Exponent of metabolic costs
q	0.8	−	Exponent of volumetric search rate
h	0.25	−	Ratio of maturation size to maximum size
μ	0.84	g/year	Scaled background mortality
ξ	0.1	−	Fraction of energy reserves
w_0	0.0005	−	Scaled egg size
f_0	0.6	−	Initial feeding level
γ	$\frac{f_0 h \beta^{2-\lambda} w_r}{\sqrt{2\pi(1-f_0)\kappa_0 \sigma}}$	g/year	Scaled factor of volumetric search rate
w_r	1	g	Reference weight for scaling[a]
κ_0	0.005	g^{-1}/m^3	Scaled magnitude of resource size spectrum
m_{cut}	0.5	−	Upper limit of resource spectrum
λ	2+q-n	−	Slope of resource spectrum
r	4	1/yr	Scaled resource generate rate

[a]For convenience, individual body size is scaled with a reference size. The remaining parameters are from Hartvig et al. (2011)

Table S5: Life history elements of the single–patch vegetation model

No.	Equation	Interpretation
N1	$\omega(m) = m/\phi$	Leaf area
N2	$h(m) = \alpha_1 \omega^{\beta_1}$	Height
N3	$m_s(m) = \rho\eta_c/\theta_\omega h$	Mass of sapwood
N4	$m_b(m) = b m_s(m)$	Mass of bark
N5	$m_h = \rho\eta_c\alpha_2\omega^{\beta_2}$	Mass of heartwood
N6	$m_r = \alpha_3\omega$	Mass of fine roots
N7	$q = 2\eta(1 - z^\eta h^{-\eta})z^{\eta-1}h^{-\eta}$ if $z \le h$, otherwise 0	Probability density of leaf area at height z for an individual of height *h*
N8	$Q = \int_z^h q(z', h)dz'$ if $z \le h$, otherwise 0	Fraction of leaf area above height *z* for an individual of height *h*
N9	$E(t) = \exp(-c_{\text{ext}} \int_0^\infty Q\big(z, h(m)\big)\omega(m)U(m,t)dm)$	Canopy openness at height *z*
N10	$A = \omega(m) \int_0^{h(m)} A_{lf}(A_0\nu, E(z,t))q(z, h(m))dz$	Gross annual CO_2 assimilation
N11	$R = \omega(m)\nu c_{R,1} + \frac{m_s(m) + 2m_b(m)}{\rho} c_{R,s} + m_r(m)c_{R,r}$	Total maintenance respiration
N12	$T = m\big(\alpha_4\phi^{-\beta_4}\big) + m_b(m)k_b + m_r(m)k_r$	Total turnover
N13	$P = c_{bio}Y(A(m,E) - R(m) - T(m))$	Net production
N14	$g(m,E) = \max\left\{\frac{\big(1 - r(m)\big)P(m,E)\mathrm{d}m}{\mathrm{d}m_t}, 0\right\}$	Growth of leaf mass
N15	$b(m,E) = \max\left\{\frac{\pi_0\pi_1}{c_{\text{ass}}s} r(m)P(m,E), 0\right\}$	Birth rate
N16	$r(m) = c_{r1}(1 + \exp(c_{r2}(1 - h(m)/h_m)))$	Fraction of production allocation to reproduction
N17	$\frac{\mathrm{d}m}{\mathrm{d}m_t} = \left(1 + \frac{\mathrm{d}m_s}{\mathrm{d}m} + \frac{\mathrm{d}m_b}{\mathrm{d}m} + \frac{\mathrm{d}m_h}{\mathrm{d}m} + \frac{\mathrm{d}m_r}{\mathrm{d}m}\right)^{-1}$	Fraction of whole-plant growth that is leaf
N18	$\pi_1 = \left(\left(\frac{P(s,E)}{\omega(s)}\right)^{-2} c_{s0}^2\right)^{-1}$ if $P(s,E) > 0$, otherwise 0	Survival of seedlings during germination
N19	$\mu(m,E) = c_{\text{d}0}\exp(-c_{\text{d}1}\rho) + c_{\text{d}2}\exp(-c_{\text{d}3}P(m,E)/\omega(m))$	Mortality rate

Table S6: Parameter values of the single-patch vegetation model

Parameter	Value	Unit	Description
ϕ	0.11	kg m^{-2}	Leaf mass per unit area[a]
ρ	608	kg m^{-2}	Stem tissue density[a]
h_m	12	m	Height at maturation[a]
s	3.8×10^{-5}	kg	Seed size
c_{ext}	0.5	-	Light extinction coefficient
η	12	-	Crown-shape parameter
η_c	$1-\frac{2}{1+\eta}+\frac{1}{1+2\eta}$	-	Stem-volume adjustment due to crown shape
θ	4669	-	Leaf area per sapwood area
α_1 β_1	5.44, 0.306	m^{-1}, -	Parameters describing scaling of height with leaf area
α_2, β_2	6.67×10^{-5}, 1.75	m, -	Parameters describing scaling of heartwood volume with leaf area
α_3	0.07	kg m^{-2}	Parameter describing scaling of root mass with leaf area
b	0.17	-	Ratio of bark area to sapwood area
υ	1.87×10^{-3}	kg m^{-2}	Nitrogen mass per leaf area
A_0	1.78×10^{5}	mol yr^{-1} kg^{-1}	Ratio of light-saturated CO_2 assimilation rate to leaf nitrogen mass
$c_{R,1}$	2.1×10^{4}	mol yr^{-1} kg^{-1}	Raito of leaf dark respiration to leaf nitrogen mass
$c_{R,r}$	217	mol yr^{-1} kg^{-1}	Fine-root respiration per mass
$c_{R,s}$	4012	mol yr^{-1} kg^{-1}	Sapwood respiration per stem volume
Y	0.7	-	Yield; ratio of carbon fixed in mass per carbon assimilated
c_{bio}	2.45×10^{-2}	kg mol^{-1}	Constant converting assimilated CO_2 to dry mass
α_4 β_4	2.86×10^{-2}, 1.71	m^2 kg^{-1} yr-1, -	Parameters describing scaling of turnover rate for leaf with ϕ
k_b	0.2	yr^{-1}	Turnover rate for bark
k_r	1.0	yr^{-1}	Turnover rate for fine roots
c_{acc}	4.0	-	Accessory costs of seed production
c_{r1}	1.0	-	Maximum allocation to reproduction
c_{r2}	50	-	Parameter determining rate of change in $r(m)$ around h_m
π_0	0.25	-	Survival probability during dispersal
c_{s0}	0.1	kg m^{-2} yr^{-1}	Parameter influencing survival through germination
c_{d0}	0.52	yr^{-1}	Baseline rate for intrinsic mortality
c_{d1}	6.5×10^{-3}	m^3 kg^{-1}	Risk coefficient for tissue density in intrinsic mortality
c_{d2}	5.5	yr^{-1}	Baseline rate for growth-rated mortality
c_{d3}	20.0	yr m^2 kg^{-1}	Risk coefficient for dry-mass production per unit leaf area in growth-related mortality

[a]Reflecting the average of trees, obtained from personal communication with D.S. Falster. The remaining parameters are from Falster et al. (2010).

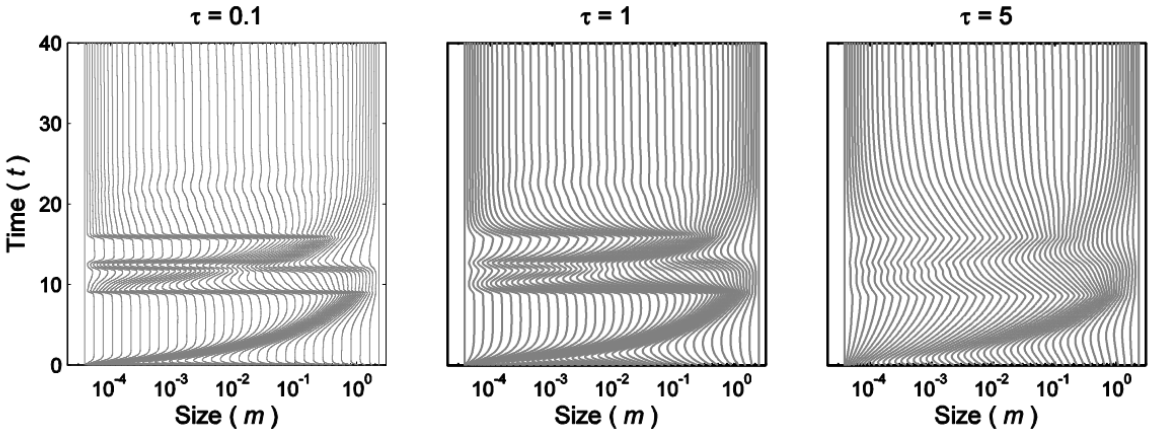

Fig. S3: Mesh trajectories for various temporal smoothing parameter τ generated by the moving-mesh upwind method for the vegetation model with 50 size classes. The density-biomass monitor function (Eq. S4b) was used.

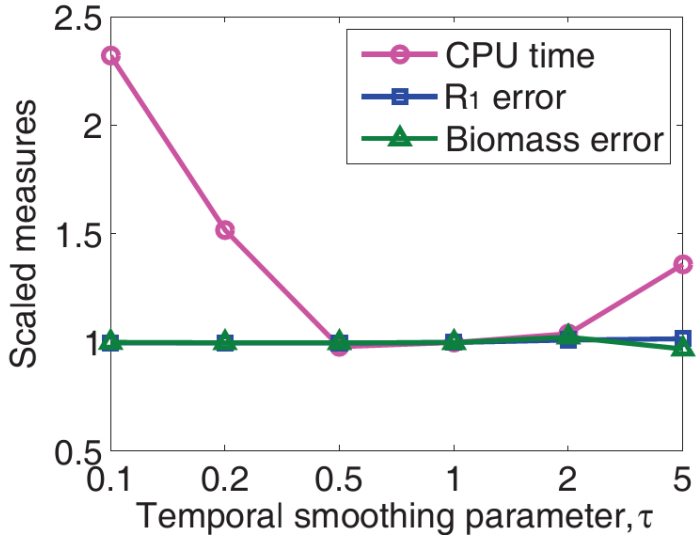

Fig. S4: Computational performance for various temporal smoothing parameter τ in the moving-mesh upwind method with 50 size classes. The R_1 norm error and population biomass error are defined by equations (2). The vegetation model with density-biomass monitor function (Eq. S4b) was used. Measures were scaled with the value at $\tau = 1$.

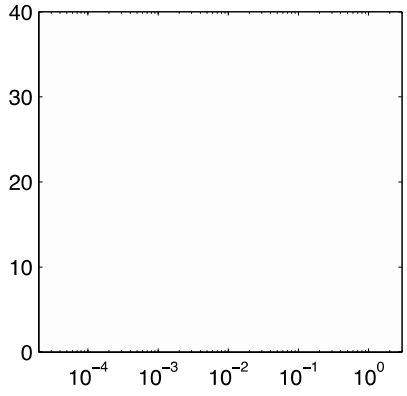

Fig. S5: Influence of density monitor function (Eq. S4a) and density-biomass monitor function (Eq. S4b) on mesh trajectory (top panels), density-size distribution (middle panels), and biomass-size distribution (bottom panels) with 50 size intervals. Solid and dotted curves indicate reference and computed solutions for the vegetation model (see results section), respectively. It is easy to see that the density monitor concentrates excessive points around the offspring size but largely ignores the peak arising at the largest size in the biomass-size distribution, which is overcome by the density-biomass monitor function.

Appendix S10: Numerical performance of the characteristic method for the fish model

The numerical performance of the characteristic method for the fish model is summarized in Fig. S6. It is easy to see that this method has poor performance in solving the fish model, primarily because the sharp change in the size distribution (Fig. S6A) causes fairly large numerical errors in the approximation of the gradient in the growth rate. Increasing the number of characteristic curves (Fig. S6B and Fig. S6C) is not really helpful since the computational time increases accordingly.

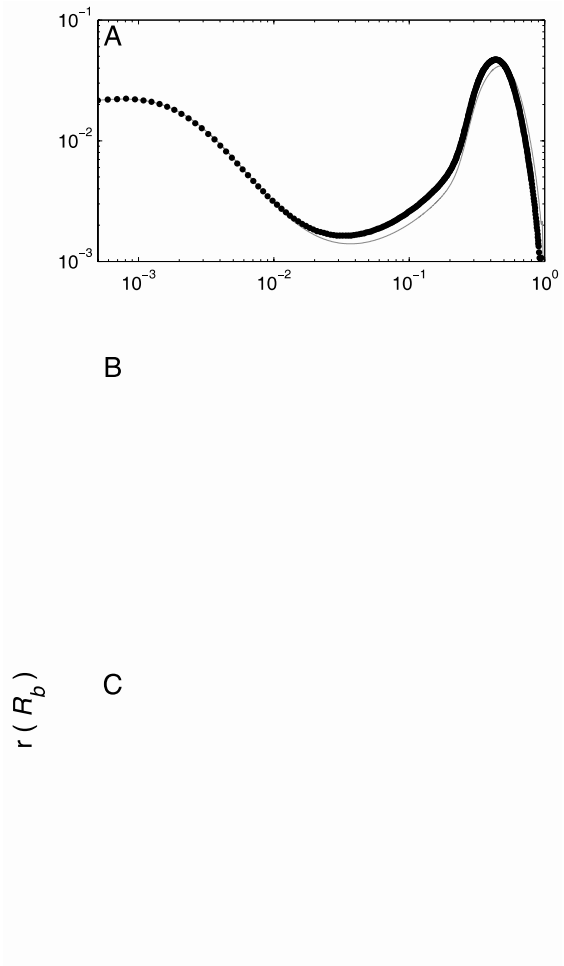

Fig. S6: (A) An example of computed (dots) equilibrium solution of the fish model using the characteristic method with 400 characteristic curves, relative to the reference equilibrium (solid curve). (B) Total error in the size distribution ($\mathbf{R_1}$), and (C) error in the population biomass ($\mathbf{R_b}$) are plotted against the used CPU time for the fixed-mesh upwind method (FMU), the moving-mesh upwind method (MMU), and the Escalator Boxcar Train (EBT) method and the characteristic method (CM). Markers indicate the number of mesh points/cohorts: 25 (square), 50 (diamond), 100 (triangle), 200 (circle), and 400 (star).

Appendix S11: An analytically tractable test model without ecological interpretation

Here, we demonstrate the computational performance of the four numerical methods on a SSPM whose life-history functions possess high regularity. Specifically, we show that the characteristic method performs satisfactorily although this is not the case for the three reference problems in the main text.

The test model here comes from Angulo and Lopez-Marcos (2004) and has the following life-history functions

$$
\begin{aligned}
g(x,t) &= 0.225(1-x^2)\frac{E}{1+E^2}\frac{t\left(1+\left(0.16+0.22e^{-0.225t^2}\right)^2\right)}{0.16+0.22e^{-0.225t^2}}\ , \\
\mu(x,t,E) &= 1.35t\frac{E}{0.16+0.22e^{-0.225t^2}}, \\
\beta\,(x,t,E) &= 0.225tx^2(1-x^2)\frac{E}{(1+E)^2}\frac{\left(0.16+0.22e^{-0.225t^2}\right)^2}{0.16+0.22e^{-0.225t^2}} \\
&\quad\times\frac{1+e^{-0.225t^2}}{61-88\log(2)+(38\log(2)-79/3)e^{-0.225t^2}} \\
E(t) &= \int_0^{1/3} u(t,x)dx+\int_{1/3}^{2/3}(2-3x)^3(54x^2-27x+4)u(t,x)dx,
\end{aligned}
\tag{S10}
$$

where $g(x,t)$ is the growth rate, $\mu(x,t)$ is the mortality rate, and $\beta(x,t)$ is the birth rate. The $E(t)$ stands for the environment reflecting the dependence of life-history functions on the density distribution.

This model is artificially designed and thus does not encompass any biological background. It has the following time-dependent analytical solution

$$u(x,t)=\frac{(1-x)^2}{(1+x)^4}+\frac{1-x}{(1+x)^3}e^{-0.225t^2},$$

when given the following initial condition

$$u(x,0)=\frac{(1-x)^2}{(1+x)^4}+\frac{1-x}{(1+x)^3}.$$

It is clear to see from Fig. S7 that all methods can produce fairly good approximation of the equilibrium solution. The efficiency diagram (Fig. S8) further shows that the characteristic method is the most efficient in terms of size-distribution error (R_1) and the second most efficient in terms of biomass error (R_b). Also for the other measures, the characteristic method works very well as shown in Table S7.

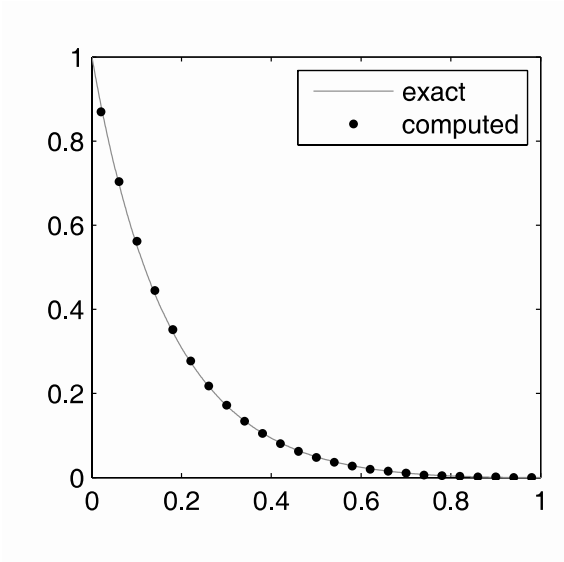

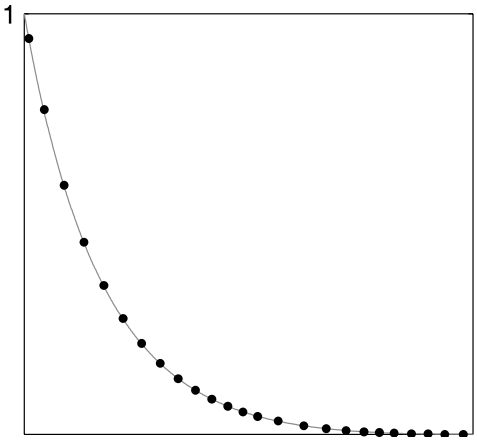

Fig. S7: Computed (dots) equilibrium solutions using methods of GMU, MMU ($\boldsymbol{\tau = 1}$), Characteristic, and the EBT with 25 computational meshes, relative to the analytical equilibrium (solid curves).

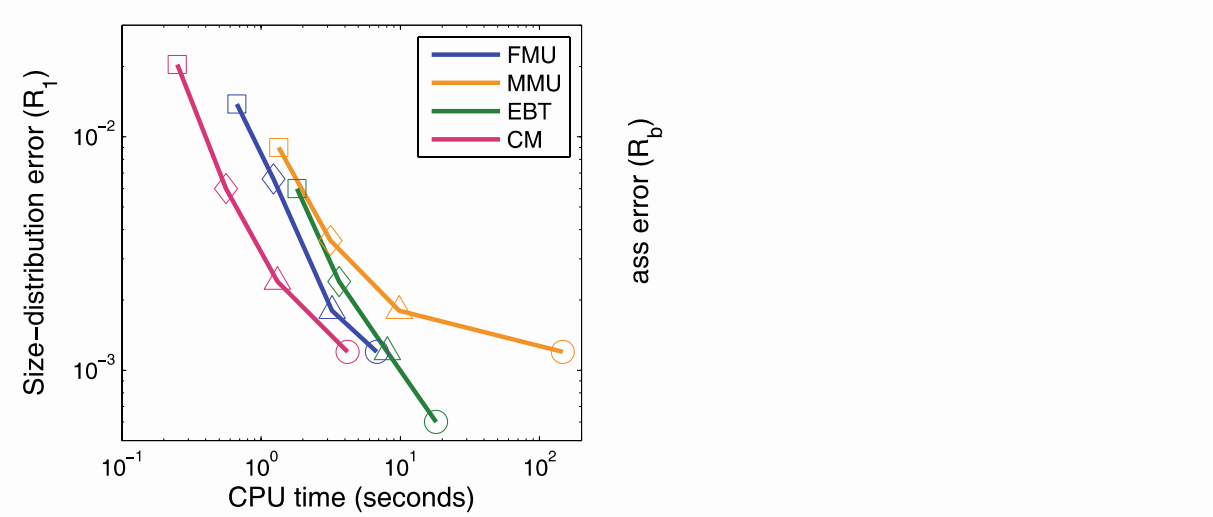

Fig. S8: Performance for the test model (Eq.S10) as measured by numerical accuracy and computational requirements. Total error in the size distribution ($\mathbf{R_1}$; left panels) and error in the population biomass ($\mathbf{R_b}$; right panel) are plotted against the used CPU time for the fixed-mesh upwind method (FMU), the moving-mesh upwind method (MMU), the characteristic method (CM), and the Escalator Boxcar Train (EBT) method. The CPU time required for tracking the cohort boundaries in the EBT method is excluded from the shown CPU times. Markers indicate the number of mesh points/cohorts: 25 (square), 50 (diamond), 100 (triangle), and 200 (circle).

Table S7: Computational efficiency for model (Eq. S10)

Mesh number	CPU time (seconds)	R_∞ error	R_1 error	Abundance error	Biomass error	Mean size error	Reproduction error
Fixed-mesh upwind method							
25	0.67	0.0176	0.0138	0.0036	0.0038	0.0002	0.0054
50	1.23	0.0068	0.0066	0.0015	0.0018	1.6e-5	0.0021
100	3.24	0.0014	0.0018	0.0009	0.0009	1.2e-5	0.0015
200	6.77	0.0010	0.0012	0.0004	0.0004	0.6e-5	0.0006
Moving-mesh upwind method							
25	1.34	0.0087	0.0090	0.0056	0.0054	0.0003	0.0105
50	3.15	0.0038	0.0036	0.0026	0.0023	0.0002	0.0048
100	9.83	0.0019	0.0018	0.0015	0.0014	0.0001	0.0027
200	147.81	0.0013	0.0012	0.0012	0.0012	3.0e-5	0.0020
Characteristic method							
25	0.25	0.0219	0.0204	0.0255	0.0145	0.0107	0.0455
50	0.56	0.0062	0.0060	0.0073	0.0040	0.0033	0.0123
100	1.31	0.0023	0.0024	0.0026	0.0018	0.0008	0.0043
200	4.18	0.0014	0.0012	0.0015	0.0013	0.0003	0.0025
Escalator Boxcar Train method							
25	1.81	0.0075	0.0060	0.0033	0.0070	0.0037	0.0081
50	3.64	0.0027	0.0024	0.0016	0.0026	0.0010	0.0039
100	8.08	0.0015	0.0012	0.0012	0.0015	0.0003	0.0021
200	18.05	0.0012	0.0006	0.0011	0.0012	0.0001	0.0019

Comparison of the computed equilibrium solution between different numerical approaches for various computational grids. Definitions of the errors are given by equations (2).

Appendix S12: Computational performance of the numerical methods

The numerical errors defined in equations (2) as well as the required computational time for different cohort numbers are reported in Table S8 (Daphnia model), Table S9 (fish model) and Table S10 (vegetation model).

Table S8: Computational efficiency for the Daphnia model

Mesh number	CPU time (seconds)	R_∞ error	R_1 error	Abundance error	Biomass error	Mean size error	Reproduction error
Fixed-mesh upwind method							
25	1.29	0.0747	0.2194	0.0282	0.0147	0.0131	0.0009
50	2.68	0.0427	0.1274	0.0103	0.0056	0.0047	0.0030
100	6.38	0.0474	0.0456	0.0036	0.0020	0.0016	0.0028
200	15.65	0.0126	0.0137	0.0033	0.0017	0.0015	0.0001
400	128.28	0.0049	0.0059	0.0014	0.0007	0.0006	0.0001
800	303.26	0.0042	0.0040	0.00060	0.0003	0.0002	0.0001
Moving-mesh upwind method							
13	1.19	0.0150	0.4934	0.0014	0.0003	0.0014	0.0014
25	2.29	0.0294	0.1645	0.0006	0.0002	0.0005	0.0007
50	4.29	0.0551	0.0406	0.0005	0.0001	0.0004	0.0005
100	61.37	0.0248	0.0105	0.0002	5.8e-5	0.0002	0.0002
200	300.37	0.0166	0.0046	0.0001	3.0e-5	0.0001	0.0001
Escalator Boxcar Train method							
13	1.93	0.0101	0.0056	1.61e-4	3.61e-4	2e-4	3.93e-5
25	2.51	0.0033	0.0021	2.90e-5	9.46e-5	6.56e-5	4.72e-5
50	5.66	0.0008	0.0005	1.06e-5	3.13e-5	2.07e-5	2.83e-5
100	11.28	0.0002	0.0001	3.76e-6	1.03e-5	6.50e-6	1.23e-5
200	24.94	0.00009	0.00004	5.71e-7	2.61e-6	2.04e-6	3.22e-6
400	282.23	0.00005	0.00002	1.46e-6	4.79e-7	1.94e-6	3.42e-6

Comparison of computed equilibrium solution between different numerical approaches for various grid numbers. Definitions of errors are given by equations (2). For the EBT method an additional set of ODEs was added to track cohort boundaries, which makes R_∞ error and R_1 error available, but the CPU time presented in the table excludes the time of calculating cohort boundary.

Table S9: Computational efficiency for the fish model

Mesh number	CPU time (seconds)	R_∞ error	R_1 error	Abundance error	Biomass error	Mean size error	Reproduction error
Fixed-mesh upwind method							
25	22.12	0.0715	0.0920	0.1390	0.1564	0.0201	0.0821
50	40.25	0.0169	0.0266	0.0543	0.0508	0.0037	0.0298
100	124.47	0.0042	0.0099	0.0204	0.0152	0.0052	0.0678
200	845.57	0.0015	0.0044	0.0081	0.0056	0.0025	0.0781
400	4387.26	0.0001	0.0028	0.00309	0.0025	0.0006	0.0815
Moving-mesh upwind method							
25	53.82	0.1206	0.1776	0.1452	0.1135	0.0372	0.0184
50	124.18	0.0305	0.0491	0.0393	0.0701	0.0321	0.0058
100	1217.18	0.0081	0.0125	0.0044	0.0115	0.0071	0.0715
200	11965.04	0.0016	0.0046	0.0001	0.0027	0.0028	0.0813
Escalator Boxcar Train method							
25	18.61	0.0194	0.0466	0.0062	0.0039	0.0086	0.0294
50	123.51	0.0076	0.0096	0.0031	0.0011	0.0035	0.0006
100	1165.48	0.0016	0.0029	0.0010	0.0006	0.0017	0.0007
200	3071.22	0.0002	0.0022	0.0008	0.0002	0.0015	0.0006

Table description is the same as Table S1.

Table S10: Computational efficiency for the vegetation model

Mesh number	CPU time (seconds)	R_∞ error	R_1 error	Abundance error	Biomass error	Mean size error	Reproduction error
Fixed-mesh upwind method							
25	11.03	0.0709	0.2194	0.149803	0.009368	0.165179	0.162799
50	13.22	0.0581	0.1274	0.011151	0.000808	0.011828	0.018795
100	34.28	0.0289	0.0456	0.016304	0.000476	0.015574	0.003758
200	142.85	0.0137	0.0137	0.008172	0.000318	0.007797	0.003724
400	976.78	0.0071	0.0059	0.004523	0.000173	0.004330	0.002391
800	13833.80	0.0065	0.0040	0.003349	0.000122	0.003216	0.001851
Moving-mesh upwind method							
13	32.7	0.0621	0.2005	0.420410	0.016566	0.696774	0.307611
25	54.49	0.0427	0.1646	0.032075	0.003228	0.029802	0.045461
50	100.94	0.0216	0.0300	0.017379	0.000380	0.016708	0.004393
100	766.89	0.0072	0.0079	0.006524	0.000149	0.006333	0.002595
200	45421.49	0.0067	0.0045	0.003956	0.000120	0.003821	0.001946
Escalator Boxcar Train method							
13	211.79	0.1483	0.4934	0.6340	0.1602	1.7035	0.5803
25	680.37	0.0557	0.1645	0.1819	0.0115	0.3824	0.0787
50	3946.21	0.0228	0.0406	0.0802	0.0069	0.1876	0.0125
100	20161	0.0065	0.0105	0.0509	0.0043	0.0927	0.0098
200	99448	0.0058	0.0046	0.0041	0.0021	0.0042	0.0021

Table description is the same as Table S1.

Appendix S13: Robustness for transient dynamics

Here we test the computational performance of the four numerical methods in solving SSPMs with respect to transient dynamics. We first determine reference solutions by integrating the representative SSPMs for a limited time such that their solutions are far from steady states, $t = 20$ (Daphnia model), $t = 1$ (fish model), and $t = 40$ (vegetation model) using the fixed-mesh upwind (FMU) method with 4000 size classes and a smooth initial condition. For the fish and vegetation model, the initial condition is obtained as a perturbation of the steady state u_s, specifically,

$$u(x,0) = u_s(x)e^{-8\left(\frac{x-x_b}{x_m-x_b}\right)^3}.$$

This initial condition is intended to represent plausible change in the size structure caused by harvesting of large individuals. For the Daphnia model, since the density at the maximally realized body size is infinite, we instead use the following initial condition

$$u(x,0) = e^{-8\left(\frac{x-x_b}{x_m-x_b}\right)^3}.$$

Consistent with the conclusion that the characteristic method fails to provide accurate approximation of the steady state solution for the three representative SSPMs, we find that it does not work well for transient solution either. Hence we focus below on the other three methods.

We compare the reference solutions with the numerical solutions obtained from the considered numerical methods using 100 size classes (Fig. S9), and the computational efficiency with respect to the R_1 and R_b errors (Fig. S10). These figures show that the EBT method remains the best choice for the Daphnia and fish models but not for the vegetation model and that the EBT and MMU methods perform better than the FMU method at capturing sharp peaks in the Daphnia and fish models. We also tried three other time instances for each model, and found that the results are qualitatively the same. Finally we considered the time-integrated

ecological measures for our models. Figure S11 shows the time-integrated relative error in population biomass change for the considered numerical methods. We find that the EBT method performs best for the Daphnia and fish model but not for the vegetation model for which the FMU method performs best. The computational performance in terms of other time-integrated ecological measures is similar.

In summary, we conclude that our results from comparing stationary solutions remain qualitatively robust when considering transient dynamics.

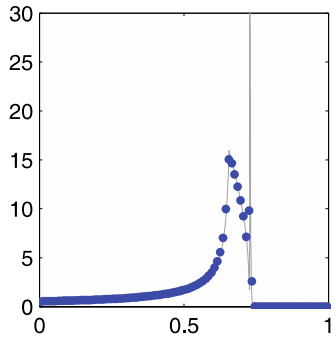

size

Fig. S9: Transient solutions at times t = 15 (Daphnia model), t = 1 (fish model), and t = 20 (vegetation model). The solid curves are the reference solutions obtained with the FMU method using 4000 size classes, while the dotted lines are the numerical solutions with 100 size classes.

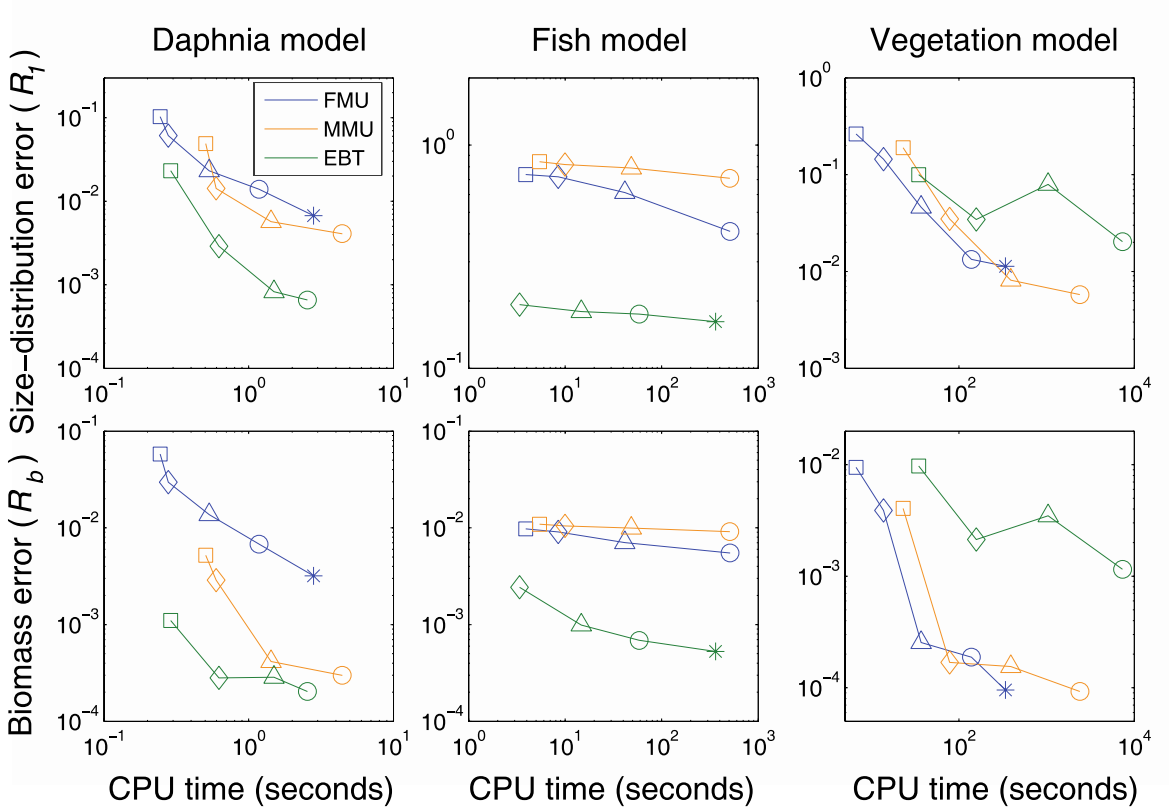

Fig. S10: Performance for the three reference problems for transient solutions as measured by numerical accuracy and computational requirements. Total relative error in the size distribution (R_1; top panels) and relative error in the population biomass (R_b; bottom panels) are plotted against the used CPU time for the fixed-mesh upwind method (FMU), the moving-mesh upwind method (MMU), and the Escalator Boxcar Train (EBT) method. Markers indicate the number of mesh points/cohorts: 13 (cross), 25 (square), 50 (diamond), 100 (triangle), 200 (circle), 400 (star).

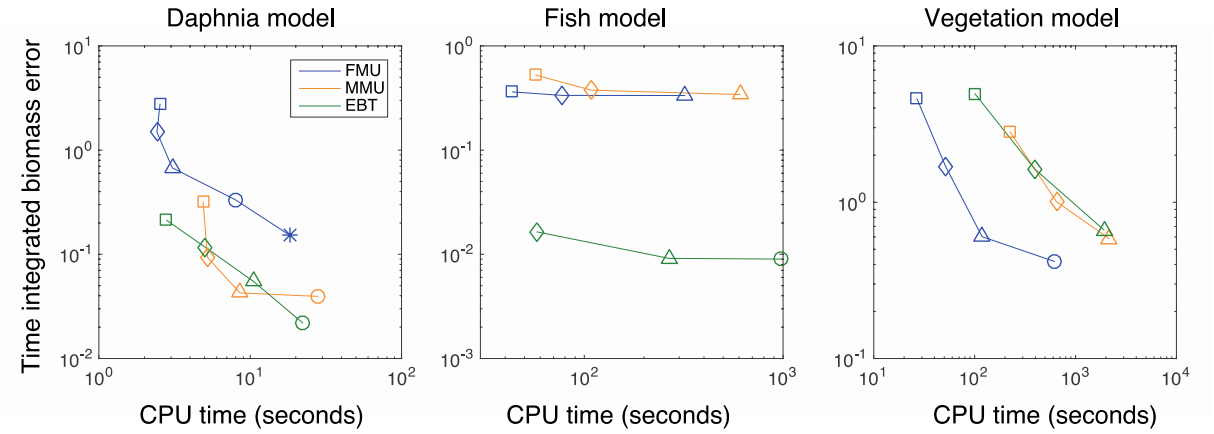

Fig. S11: Performance for the three reference problems for transient solutions as measured by numerical accuracy and computational requirements. Time integrated relative error in the population biomass ($\int R_\mathrm{b}\mathrm{d}t$) is plotted against the used CPU time for the fixed-mesh upwind method (FMU), the moving-mesh upwind method (MMU), and the Escalator Boxcar Train (EBT) method. Markers indicate the number of mesh points/cohorts: 13 (cross), 25 (square), 50 (diamond), 100 (triangle), 200 (circle), 400 (star). The integration times are 150 (Daphnia model), 10 (fish model) and 100 (vegetation model) with the initial condition as specified in this section.

References

[1] Angulo O., Lopez-Marcos J.C. 2002. Numerical integration of autonomous and non-autonomous non-linear size-structured population models. Mathematical Biosciences 177, 39-71.

[2] Angulo O., Lopez-Marcos J.C., 2004. Numerical integration of fully nonlinear size-structured population models. Applied Numerical Mathematics 50, 291-327.

[3] de Boor C., 1973. Good approximation by splines with variable knots II, in Springer Lecture Notes Series 363, Springer-Verlag, Berlin.

[4] de Roos A. 1988. Numerical methods for structured population models: the escalator boxcar train. Numerical Methods for Partial Differential Equations 4, 173-195.

[5] de Roos A.M., Metz J.A.J., Evers E., Leipoldt A., 1990. A size dependent predator-prey interactions: who pursues whom? Journal of Mathematical Biology 28, 609-643.

[6] de Roos A.M., Diekmann O., Metz J.A.J., 1992. Studying the dynamics of structured population models: A versatile technique and its application to Daphnia. American Naturalist 139, 123-147.

[7] Falster D.S., Brännström Å., Dieckmann U., M., Westoby, 2010. Influence of four major plant traits on average height, leaf-area cover, net primary productivity, and biomass density in single-species forests: a theoretical investigation. Journal of Ecology 99, 148-164.

[8] Hartvig M., Andersen K.H., Beyer J.E., 2011. Food web framework for size-structured populations. Journal of Theoretical Biology 272, 113-122.

[9] Huang W.Z., Ren Y.H., Russell R.D., 1994. Moving mesh partial differential equations (MMPDES) based on the equidistribution principle. SIAM Journal on Numerical Analysis 31, 709-730.

[10] Huang W.Z., Russell R.D., 2011. Adaptive moving mesh methods. In Springer Applied Mathematical Sciences Series 197, Springer-Verlag, Berlin.

[11] Kooijman S.A.L.M., Metz J.A.J., 1984. On the dynamics of chemically stressed populations: the deduction of population consequences from effects on individuals. Ecotoxicology and Environmental Safety 8, 254-274.

[12] Leonard B.P., 1979. A stable and accurate convective modelling procedure based on quadratic upstream interpolation. Computational Methods Applied in Mechanical Engineering 19, 59-98.

[13] LeVeque R.J., 2002. Finite Volume Methods for Hyperbolic Problems. Cambridge University Press.

[14] Patankar S.V., 1980. Numerical Heat Transfer and Fluid Flow. Taylor & Francis. ISBN 978-0-89116-522-4.

[15] Roe P.L., 1986. Characteristic-based schemes for the Euler equations. Annual Review of Fluid Mechanics 18, 337-365.

[16] Stockie J.M., MacKenzie, J.A., Russel R.D., 2001. A moving mesh method for one dimensional hyperbolic conservation laws. SIAM Journal on Scientific Computing 22, 1791-1813.

[17] Sweby P.K., 1984. High resolution schemes using flux limiters for hyperbolic conservation laws. SIAM Journal on Numerical Analysis 21, 995-1011.